Age-related decline in prefrontal glutamate predicts failure to efficiently deploy working memory in the service of learning

Milena Rmus[1], Mingjian He[2], Beth Baribault[1], Edward G. Walsh[3], Elena K. Festa[3], Anne G.E. Collins[1], and Matthew R. Nassar[3]

[1]UC Berkeley
[2]Massachusetts Institute of Technology
[3]Brown University

February 9, 2023

Abstract

The ability to use past experience to effectively guide decision making declines in older adulthood. Such declines have been theorized to emerge from either impairments of striatal reinforcement learning systems (RL) or impairments of recurrent networks in prefrontal and parietal cortex that support working memory (WM). Distinguishing between these hypotheses has been challenging because either RL or WM could be used to facilitate successful decision making in typical laboratory tasks. Here we investigated the neurocomputational basis for age-related decision making deficits using an RL-WM task to disentangle these mechanisms, a computational model to quantify them, and magnetic resonance spectroscopy to link them to their molecular bases. Our results reveal that learning declines in older age are largely attributable to working memory deficits, as might be expected if cortical recurrent networks were unable to sustain persistent activity across multiple trials. Consistent with this, we show that older adults had lower levels of prefrontal glutamate, the excitatory neurotransmitter thought to support persistent activity, compared to younger adults. Individuals with the lowest prefrontal glutamate levels displayed the greatest impairments in working memory after controlling for other anatomical and metabolic factors. Together, our results suggest that reductions in prefrontal glutamate across healthy aging may contribute to failures of working memory systems and impaired decision making in older adulthood.

1 Introduction

People and animals undergo a number of cognitive changes across healthy aging, and while some of such changes reflect improvements emerging from an extended lifespan of continual learning, others are characterized by declines in function with advanced age (Cattell, 1943). In particular, recent work has highlighted age-related deficits in decision making under uncertainty, particularly in situations where decision outcomes are learned through experience (Eppinger et al., 2013). While such deficits could have critical importance for both aging individuals and society, the exact mechanisms underlying these deficits remain unclear. One possibility is that such impairments stem from an inability to retain the task-relevant information (i.e. working memory, Salthouse and Babcock, 1991), whereas another possibility is that such impairments stem from failures to learn state action values through reinforcement (i.e. reinforcement learning, Chowdhury et al., 2013). These different cognitive processes are supported by different neural systems. Understanding how they contribute to impairments in decision-making across lifespan could also help shed light on biological age-related mechanisms of impaired decision-making.

Previous work has shown that working memory declines with aging (Salthouse and Babcock, 1991). Such declines have been shown in both cross sectional and longitudinal studies and across a range of working memory tasks (Salthouse and Babcock, 1991). Working memory is thought to be implemented through persistent activation of neural firing in similarly tuned neurons within recurrent excitatory networks in prefrontal and parietal cortices (Andersen

and Buneo, 2002; Goldman-Rakic, 1995). Within such networks, successful maintenance of activity over a delay period depends on glutamatergic signaling, and in particular activation of NMDA receptors (Durstewitz et al., 2000; Van Vugt et al., 2020). In aged monkeys, such persistent activations in prefrontal cortex are diminished and can be restored through local pharmacological manipulations that affect intrinsic neural excitability (Wang et al., 2011). While the mechanisms by which persistent activity deteriorates with age are not fully established, observed reductions in synapses and dendritic spines on aged prefrontal pyramidal neurons (Dumitriu et al., 2010) suggest that they result at least in part from an overall reduction in glutamatergic signaling. Thus, if age-related behavioral deficits stem from diminished working memory functions, they may result from reductions in glutamate signaling in prefrontal and parietal regions that support working memory.

Reinforcement learning (RL) systems are also thought to decline across healthy aging. Evidence for such declines comes from behavioral impairments in tasks where participants learn to map stimuli onto rewarded actions (Eppinger et al., 2013; Frank and Kong, 2008; Hämmerer et al., 2011). Learning in such tasks is thought to occur through reinforcement of associations between stimulus and action in the striatum driven by dopamine reward prediction error signals (A. G. Collins and Frank, 2014; Frank et al., 2004). Such reward prediction error signals are blunted in healthy aging (Samanez-Larkin et al., 2014) supporting the accounts of age-related decline in RL (Chowdhury et al., 2013; Eppinger et al., 2013). Chowdhury et al. (2013) found that boosting dopamine signaling with dopamine precursor levodopa (L-DOPA) led to restoration of RPEs, and recovery of learning performance in older adults. The results from these studies appear to indicate that neural mechanisms underlying reinforcement learning are impaired in older adults, however a number of other studies have suggested that RL systems are intact in older adults (Grogan et al., 2019; Radulescu et al., 2016). Some of the discrepancy in these results may stem from inconsistencies in the tasks used to measure RL across different studies (Eckstein et al., 2022), as many tasks that could be solved through incremental learning in the striatum according to reward prediction errors (RL) could also be solved using other cognitive systems, working memory systems being one of particular importance (Yoo and Collins, 2022).

Typical reinforcement learning tasks require identifying the best action to choose when confronted with a given stimulus based on previous feedback. While RL models of such tasks assume that action values are learned incrementally, as if through adjustment of synaptic weights in the striatum, it is also possible for participants to achieve success on such tasks through short term storage of recent trial information in working memory. Recent work has used task designs that can dissociate these potential contributors to goal directed behavior, along with models that can quantify them, to show that behavioral deficits previously thought to reflect reinforcement learning were actually attributable to working memory systems (A. G. Collins et al., 2014). The reinforcement learning-working memory task (A. G. Collins, 2018; A. G. Collins et al., 2014; A. G. Collins and Frank, 2012, 2018) is a simple stimulus-response association learning task with a format that is commonly observed in RL studies (Frank and Kong, 2008). However, this task includes a WM manipulation - varying the number of stimulus-response actions (set size) participants need to learn. This manipulation targets WM as a capacity-limited, short term process, since increasing set-size increases both load and average duration between stimulus repetitions. Thus, varying the set size can shift contribution of RL/WM to performance and help tease apart which of the two participants are relying on when performing the task. This task has yielded important mechanistic insights into general, as well as clinical populations (A. G. Collins et al., 2014; A. G. Collins and Frank, 2012; Master et al., 2020).

In the current project, we combined cognitive, computational and neural approaches to address the question of 1) how the age-related deficits in making decisions from experience emerge from RL and WM computational mechanisms and 2) how the changes in these mechanisms relate to age-related changes in relevant neural systems. To this end, we administered an RL-WM task to young and older adults and modeled their behavior using computational model that can distinguish between deficits in RL and WM systems. We used Magnetic Resonance Spectroscopy (MRS) to measure levels of glutamate and GABA in regions thought to support working memory (prefrontal/parietal cortices) and reinforcement learning (striatum).

We found that older participants performed worse in the RL-WM task compared to young adults, and that the reduced performance was largely attributable to a more rapid decay of task relevant information in working memory. Older adults also had reduced glutamate levels, particularly in prefrontal and parietal cortices where glutamate is thought to support the persistent activation that underlies working memory. Furthermore, reductions in prefrontal glutamate were related to working memory decay across individuals - such that those with the lowest levels of prefrontal glutamate had the most rapidly decaying working memories. Taken together, our results suggest that age-related working memory declines give rise to decision making deficits that may result from failures of recurrent excitatory networks to sustain persistent representations as glutamate levels decline over healthy aging.

2 Results

42 older (age mean(SD) = 68(8.5)) and 36 younger (age mean(SD) = 21(4.4)) participants were enrolled in a two session study. Age-normed total RBANS (Randolph et al., 1998) scores were similar in both groups (mean[std] younger: 106.4 [12.0], older: 109.0[10.8]) suggesting that our cohorts reflected comparable samples of the the population with respect to overall cognitive ability. Furthermore, all participants scored in cognitively healthy range (younger adults range: 83-140; older adults range: 81-141), since cognitive impairment is defined as score 70 or below. The first session required performance of an RL-WM task designed to dissociate the contributions of working memory and reinforcement learning to decision making under uncertainty. The second study session included an MRI session in which MR spectroscopy was used to measure glutamate and GABA in key regions thought to support working memory (middle frontal gyrus [MFG] of prefrontal cortex and intraparietal sulcus [IPS]) and reinforcement learning (striatum).

In the RL-WM task, older and young adults were required to learn correct stimulus-response (key press) associations, with the goal of earning as many points as possible. After the stimulus appeared, the participants had $1s$ to make their response, following which they received deterministic feedback. Each stimulus appeared 9 times in a block, pseudo-randomly interleaved with other stimuli, allowing the participants to learn correct associations from feedback. The task has a common reinforcement-learning (RL) experiment structure (Frank et al., 2004), with an important difference: the number of associations varied (either 3 or 6) between different, fully independent blocks. This enabled us to manipulate the degree to which working memory (WM), a capacity limited system, might contribute to behavior by storing recent stimulus-action-outcome information. In particular, previous computational and empirical work using this task suggests that working memory will contribute less to decisions in the high set size condition (6 associations), but that slower learning in high set size paradoxically leads to better retention relative to learning in a surprise "test phase" in which learned associations are tested in the absence of feedback (A. G. Collins, 2018).

2.1 Behavioral results; model-independent

2.1.1 Learning

Both age groups learned to make accurate responses in the learning phase and did so more quickly in blocks with fewer interleaved stimuli, but younger adults learned more successfully than their older counterparts (Fig: 1 B&C). The learning curves reveal patterns that are consistent with RL and WM involvement in young adults (early spike in accuracy for lower set size that's absent for larger set size, that is considered a marker of fast/one-shot learning characteristic of WM but not RL; (A. G. Collins & Frank, 2012)). This pattern is less clear in older adults. Average accuracy of individuals in the young and old groups was 0.74 (SD = 0.01). and 0.60 (SD = 0.01) respectively (ANOVA for group difference: $F(1,76) = 45.42, p = 2.71e-09$). Younger adults had higher accuracy compared to older adults for both set sizes 3 ($t(76) = 4.71, p = 1.05e-05$) and 6 ($t(76) = 7.03, p = 7.61e-10$). Training performance deficits in both set sizes were greatest in the oldest individuals, as revealed by significant correlations between age and training accuracy within the older group (Fig: 1C; $r(n_S = 3\ accuracy, age) = -0.42,\ p = 0.03$; $r(n_S = 6\ accuracy, age) = -0.41,\ p = .04$).

To test what factors (i.e. set-size, reward history, delay) impact accuracy on a trial-by-trial level, we ran a mixed-effects general linear model (GLM). The GLM analysis of accuracy data indicated that both groups showed signatures of RL and WM in their behavior. We found a positive effect of reward history ($\beta = 1.74,\ t = 43.51,\ p < 0.0003$) that was apparent in both young and old groups (young: $\beta = 1.66,\ t = 27.60,\ p < 0.0003$;older: $\beta = 1.74,\ t = 32.5$,$p < 0.0003$). We also found negative effects of set size and delay on accuracy (set size: $\beta = -0.26,\ t = -9.91,\ p < 0.0003$;delay: β=-0.30, $t = -13.3,\ p < 0.0003$), that were apparent in both young (set size: $\beta = -0.23, t = -7.55,\ p < 0.0003$; delay:$\beta = -0.21,\ t = -5.11,\ p < 0.0003$) and older adults (set size: $\beta = -0.34,\ t = -9.73,\ p < 0.0003$; delay: $\beta = -0.29,\ t = -8.92,\ p < 0.0003$).

Coefficients from the GLM, particularly those capturing behavioral hallmarks of working memory (i.e. set size, delay), could be used to infer participants age. A linear regression to predict the individual participants' age based on their respective coefficients from the behavioral logistic regression model yielded negative coefficients for the accuracy fixed effect ($\beta = -17.2,\ t(71) = -5.64,\ p = 3.1455e-07$) and its sensitivity to set size ($\beta = -7.44,\ t(71) = -3.01,\ p = 0.0035$), suggesting that older adults had lower overall performance but were also more affected by the set size manipulation. Reward history coefficients took positive values ($\beta = 12.73,\ t(71) = 4.24,\ p = 6.5262e-05$) in the same model, suggesting that older adults were also more sensitive to previous rewards than their younger counterparts.

2.1.2 Testing

Both age groups experienced set size dependent declines in performance during the test phase of the task, with older adults achieving lower levels of performance overall (Fig: 1B, inset figures). Consistent with the notion that greater use of WM during learning in small set sizes weakens RL-dependent learning as expressed in the test phase (A. G. Collins, 2018), participants had greater declines in performance for set size 3 than for set size 6 between training and testing (t($\Delta_{3^L,3^T}$, $\Delta_{6^L,6^T}$) young: $t(35) = 4.64$, $p < .001$; older: $t(41) = 8.1$, $p < .001$). A 2-sample t-test revealed a trending result suggesting that the set-size based asymmetry in accuracy decline from training to testing might be greater in older adults ($t(76) = 1.62$, $p = .1$), but the effect did not reach significance.

A GLM fit to test phase accuracy confirmed that reward history was still strongly linked to performance in the test phase, but that set size was less important. An analogous mixed effect model to that used on the training data revealed positive reward history effects in both young and older adults (young: β = 1.03, $t = 16.2$, $p < .001$; older: β = .92, $t = .92$, $p < .001$). In contrast, in the test phase there was limited evidence for an effect of set size on performance in young adults ($\beta = -0.15$, $t = -1.85$, $p = .06$) and only a very modest effect in the older adults ($\beta = -0.20$, $t = -3.07$, $p = .002$).

In summary of our basic behavioral results, general patterns in the data are consistent with contributions of both working memory and reinforcement learning to behavior, replicate previous findings showing interactions between the two revealed in the test phase, and confirm age-related variability in performance. To better understand how the WM and RL mechanisms vary with age, we used computational modeling to further dissect the computational factors giving rise to differences in participant behavior.

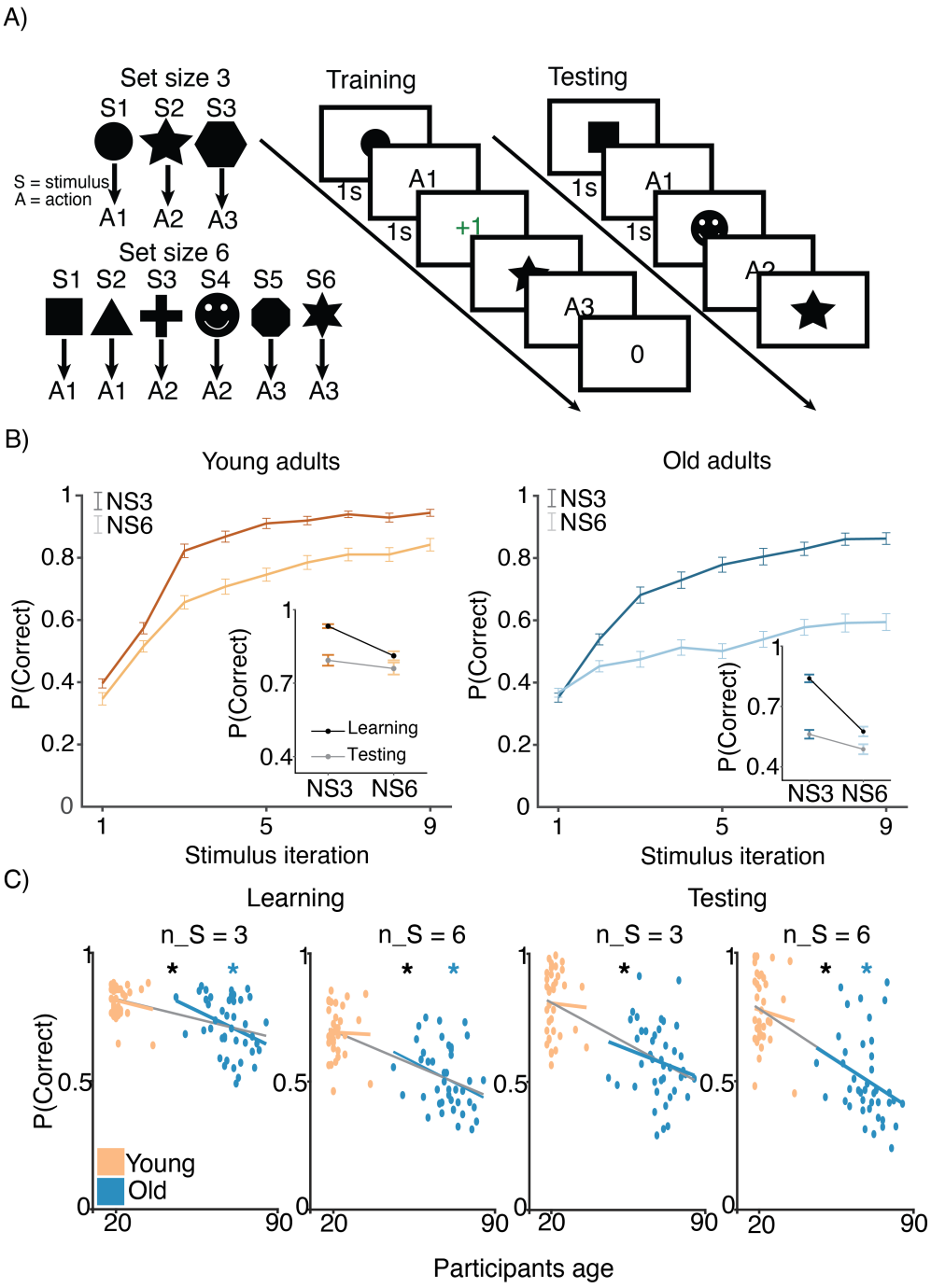

Figure 1: Experimental design. A) RL-WM task with $n_S = 3$ and $n_S = 6$ blocks. Participants learned 3 or 6 stimulus-action associations and received truthful feedback on each trial. In the test phase participants observed the same images observed during learning, and were asked to produce the responses they remembered being correct, without being given the feedback. B) Learning curves and learning/testing comparison for both set sizes in younger and older adults. Younger adults performed better overall, with smaller difference in performance between the set sizes. The older participants showed greater drop-off in set size 3 between learning and testing compared to young adults. C) Age correlations with average accuracy in each set size conditions across both learning and testing. All full sample negative correlations between age and performance were significant [gray lines]; there were no significant age-performance correlations within young age group [yellow lines]. Age and performance were significantly correlated within old group [blue] in all conditions except set size 3 in testing.

2.2 Modeling results

To get a better insight into how specific learning mechanisms vary with age, we fit a computational model to the RL-WM task behavioral data. Specifically, we applied a hybrid RL-WM model that quantifies how WM and RL contribute to learning together (Fig. 2; for a detailed description of how the model captures WM and RL processes see Methods section). Parameters attributed to WM consisted of 1) WM decay (ϕ) – capturing the rate at which stimulus-response associations decayed during learning, and 2) set-size dependent WM reliance parameters (ω^3 and ω^6) – capturing relative reliance on WM (as opposed to RL) to make choices. RL parameters consisted of the learning rate (α^+) and test phase softmax inverse temperature (β^T), governing the rate at which participants updated the stimulus-response association values based on observed feedback, and the extent to which participants' test phase choices were deterministic vs. exploratory, respectively. Learning phase softmax beta (β^L) captured the same dynamic during the learning phase (but unlike all other RL-WM model parameters was estimated at the group-level only; see Methods for details). We also incorporated a negative learning rate (α^-), to differentiate learning from negative versus positive feedback, which was present in both RL and WM modules. Finally, the model included a noise parameter in response selection (ε), to capture random lapses in task performance.

We implemented the RL-WM model in a hierarchical Bayesian framework, as Bayesian model fitting offers many statistical benefits (e.g., Kruschke & Liddell, 2018) and incorporating hierarchical structure allowed us to account for individual- and group-level effects simultaneously (among other practical benefits; e.g., Lee, 2011). As this represents a novel extension of the RL-WM model, we offer full model specification across the Methods section and Supplement; further details on the exact approach to Bayesian model fitting are also available in Methods.

2.2.1 Model comparison

We first compared the performance among the three versions of our Bayesian RL-WM model (with different hierarchical structures; see Methods for details) in order to select a model to use in all model-based analyses of our data. Our model comparison indicated that the "two-group" version of the model, which incorporated separate hierarchies over the participants within each age group, offered the best description of our data (see Fig. S2). This two-group, hierarchical version of the model outperformed both the non-hierarchical model ($\Delta\text{WAIC} = 1.62 \times 10^3$) and the model that included a single hierarchy over all participants, regardless of their age group ($\Delta\text{WAIC} = 1.86 \times 10^2$). This model's posterior predictive learning curves and posterior predictive asymptotic means (Fig. 2B) successfully captured the general patterns in performance of both age groups on the RL-WM task.

2.2.2 Parameter analysis

We next examined which parameters of the model differed substantially across age groups. The strongest difference between the age groups was with respect to decay rate ϕ in the WM module. The group mean decay rate was much higher in the older age group ($\Delta\,\mu^\phi = -0.151$, 95% equal-tailed credible interval (CrI) $= [-0.227, -0.070]$) indicating that the stimulus-action-outcome associations stored in WM degraded faster for older adults. Mean decay rate for the younger group was 0.174, indicating that an association would decay to 83% of its original strength after a single trial, whereas in older adults the decay of 0.324 would lead to working memory degradation about twice as fast.

Next, we focused on the relative WM reliance parameter ω. We were interested in exploring whether the WM reliance might follow the similar pattern observed in group-related difference in the WM decay. For instance, if older participants' WM module is markedly more forgetful, they would accordingly rely less on the association weights stored in WM to guide their action selection. In our analysis, we observed that the relative reliance on WM over RL — as captured by the set-size dependent policy mixture parameters ω^{ns} — depended heavily on the set size in both groups. While learning stimulus-action associations in set size 3, participants in both groups relied more on WM ($\omega^3 > 0.5$ for 36 of 36 younger and 40 of 42 older participants). In set size 6, participants in both groups tended to rely more on RL ($\omega^6 < 0.5$ for 32 of 36 younger and 35 of 42 older participants). Importantly, ω^3 was greater than ω^6 for 36 of 36 younger and 40 of 42 older participants. We observed the same effect for the group mean parameters, with similar magnitudes for both groups ($\mu^{\omega^3} - \mu^{\omega^6}$, young: $[0.336, 0.549]$; older: $[0.214, 0.420]$). Older adults had a somewhat reduced tendency to rely on WM ($\Delta\,\mu^{\omega 3} = 0.090[-0.003, 0.179]$) compared to younger adults, even when doing so is appropriate (i.e., for the smaller set size), but this difference was not robust. Thus, older and young adults showed similar patterns in WM reliance, contingent on the set-size.

The model fits revealed very little indication of group differences in parameters specific to the RL system. We found no group differences in the test phase beta β^T ($[-0.4657.673]$) or the learning rates α ($[-0.0070.042]$). Our

model did have a learning rate asymmetry parameter which affected both RL and WM systems, and allowed the model to capture a consistent trend toward higher learning from positive relative to negative outcomes in both groups. This was evident in group means ($\mu^{\alpha^+} - \mu^{\alpha^-}$, young: $[0.004, 0.049]$, older: $[0.009, 0.041]$) as well as for individual participants ($\alpha^+ > \alpha^-$ for 34 of 36 young and 42 of 42 older participants). This asymmetry differed across groups, such that negative learning rates were higher in the young adult group as compared to the older adults (Fig. 2C) ($\Delta\ \mu^{\alpha^-} = 0.016, [0.002, 0.032]$). This suggests that older adults neglected negative feedback even more relative to young adults. This result is inconsistent with the previous work suggesting that older adults exhibit bias in learning from negative outcomes (Frank and Kong, 2008). However, this finding has not been consistent across studies, and in our paradigm a bias toward learning from positive outcomes could be viewed as an adaptive strategy when resources are limited, in that positive outcomes perfectly prescribe the correct future action, whereas negative ones only rule a single response out.

Importantly, the noise/random lapse parameter did not differ between the two age groups ($\Delta\,\mu^{\varepsilon} = [-0.011, 0.047]$), which suggests it is unlikely that the observed differences in accuracy are due to older adults simply having noisier data.

To demonstrate the impact of their higher decay rate on older adults' learning, we again simulated older adults' behavior from the fitted model, except we used the young adults' group-level decay rate in place of every older adult's individual-level decay rate. To do this, we used the same procedure as was used to generate the posterior predictive plots (as in Figure 2b; see Methods), except with the aforementioned parameter swaps. This demonstration, shown in Figure S5, suggests that the older adult's higher decay rate could potentially account for most of the difference in learning behavior between the age groups.

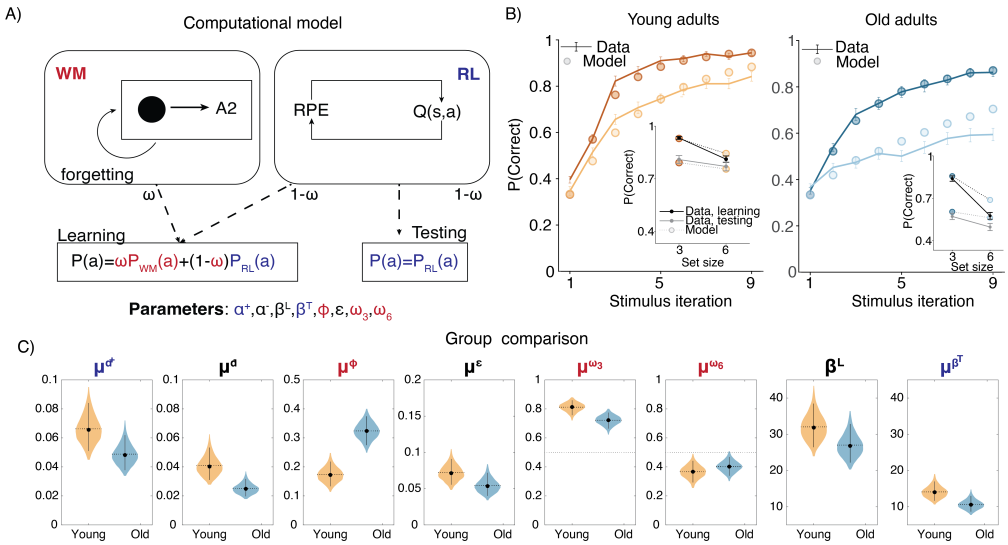

Figure 2: Computational model. A) RL-WM computational model schematic. B) Posterior predictive checks for group-level learning curves and asymptotic (last 3 stimulus iterations) means from our Bayesian RL-WM model. Darker color represents set size 3; lighter color represents set size 6. C) Comparison of group-level mean parameters shows that primarily WM parameters drive differences between young and older adults, especially the forgetting rate parameter μ^{ϕ}. Dashed lines represent equal contributions of WM and RL processes.

2.2.3 Linking MRS measures, model parameters and behavioral performance

Thus far, our results suggest that 1) there is a significant difference in performance between two age groups, and 2) that this difference is best explained by working memory deficit in older group (most significantly WM decay, and marginally reliance on WM in smaller set size condition). Next, we aimed to test how these age-related differences relate to metabolic changes affecting brain neurochemistry. We used magnetic resonance spectroscopy (MRS) to measure neurotransmitters (glutamate and GABA) that support working memory (Wong and Wang, 2006) in regions important for both reinforcement learning (Striatum [STR]) and working memory (Middle Frontal Gyrus of prefrontal

cortex [MFG], Intraparietal sulcus [IPS]). To control for larger structural changes that may covary with differences in glutamate and GABA levels, we included gray volume, white matter volume and cortical thickness (in caudal middle frontal [CMF], superior frontal [SF], and rostral middle frontal [RMF] cortex) in our analyses, and to control for non-specific metabolic changes we included measures of N-acetylaspartate (NAA).

In order to understand how differences in performance and their computational mechanisms relate to the neural measures we took a data-driven multi-step analysis approach. First, we constructed a GLM to explain overall learning performance according to structural measures collected as part of our high resolution anatomical MRI scans (white matter, gray matter, cortical thickness) as well as neurochemical measures from MRS (glutamate, GABA, NAA). Given correlations in our neurochemical measures across brain regions, we attempted to maximize power to detect relationships in our initial linear model by aggregating neurochemical measures across brain regions. Specifically, we averaged the MRS measures across regions (i.e. average glutamate was the average of glutamate measures from medial frontal gyrus, intraparietal sulcus and striatum). Anatomical specificity of significant predictors was then examined in followup analyses. We set up a linear model predicting average learning performance using the following z-scored predictors: GABA, Glutamate, NAA, gray matter, caudal middle frontal [CMF] cortical thickness, superior frontal [SF] cortical thickness and rostral middle frontal [RMF] cortical thickness (see methods for details). The best model identified through a regularized and cross-validated fitting procedure included GABA, glutamate, NAA, CMF cortical thickness and SF cortical thickness ($R^2 adjusted = .41$, $F = 7.8$, $p < .001$). However, the only coefficient within this model for which a value of zero could be reliably rejected was our aggregate measure of glutamate concentration ($\beta = .04$, $t = 2.5$, $p = .01$) (Fig 3 B).

Next, we used our best fitting model to generate brain-based predictions of performance so that we could evaluate their computational specificity. These predictions can be thought of as projections of behavioral learning performance onto the axis of brain measures most closely related to it. We then fit a linear model that regressed the brain-predicted performance onto an explanatory matrix that contained all parameter estimates from our behavioral model in order to determine which computational elements are most tightly linked to the neural fingerprint of performance (or performance failures). This model explained a significant amount variance in our brain-based performance measure ($R^2_{\text{adjusted}} = .48$, $F = 7.46$, $p < .001$) and revealed that WM decay ϕ (β = -0.02, $t = -2.24$, $p = .03$) and set size 3 WM weight ω_3 (β = .02, $t = 2.35$, $p = .03$) contributed substantially to these predictions – suggesting that the brain-based predictions largely reflected the integrity of a working memory system (Fig 3 C).

Having established that 1) glutamate contributes to accuracy, and that 2) WM parameters ϕ and ω capture the performance predictions based on glutamate (and remaining non-significant neural measures), we next tested the anatomical specificity of the glutamate-working memory relationship. To do so, we constructed two additional regression models, in which we regressed ϕ ($R^2 adjusted = .32$, $F = 9.22$, $p < .001$) and ω ($R^2 adjusted = .23$, $F = 6.42$, $p < .001$) onto three separate glutamate measures extracted from MFG, IPS and striatum. From these 2 models, the only significant coefficient was the effect of MFG glutamate on WM decay ϕ (β = -.04, $t = -2.95$, $p = .004$) (Fig 3 D). Specifically, the lower glutamate levels seemed to predict higher WM decay. This relationship was specific to glutamate, and was not observed when we substituted measures of glutamine ($r = -.05$, $p = .70$), a molecule with a nearby spectral peak. The relationship between MFG glutamate and WM memory decay persisted even after regressing out variance related to MFG gray matter [GM] and MFG creatine [Cr] ($r = -.39$, $p = .0035$), suggesting that our results are specifically related to glutamate rather than picking up on non-specific anatomical differences such as gray matter or tissue density.

Next, we examined how age factors into this relationship. We found that age negatively correlated with glutamate ($r_{\text{Spearman}} = -.59$, $p = 2.9362e-06$) and positively correlated with decay ($r_{\text{Spearman}} = .63$, $p = 3.1536e-07$). The visualization of this depicted in Figure 3D suggests that older adults have lower glutamate levels and higher decay, whereas inverse is true for younger adults. Since age was negatively correlated with glutamate and positively correlated with decay, there is a possibility that age alone could fully explain the correlation between glutamate and WM decay. To address this question, we ran a correlation between MFG glutamate and WM decay in the two age groups separately. We found that glutamate was not predictive of WM decay in young adults ($r = .11, p = .54$), but there was a trending correlation between glutamate and WM decay in older adults ($r = -.36$, $p = .08$). These results suggest that prefrontal glutamate levels decrease with aging and potentially contribute to declines in working memory that account for the majority of age-related learning impairments.

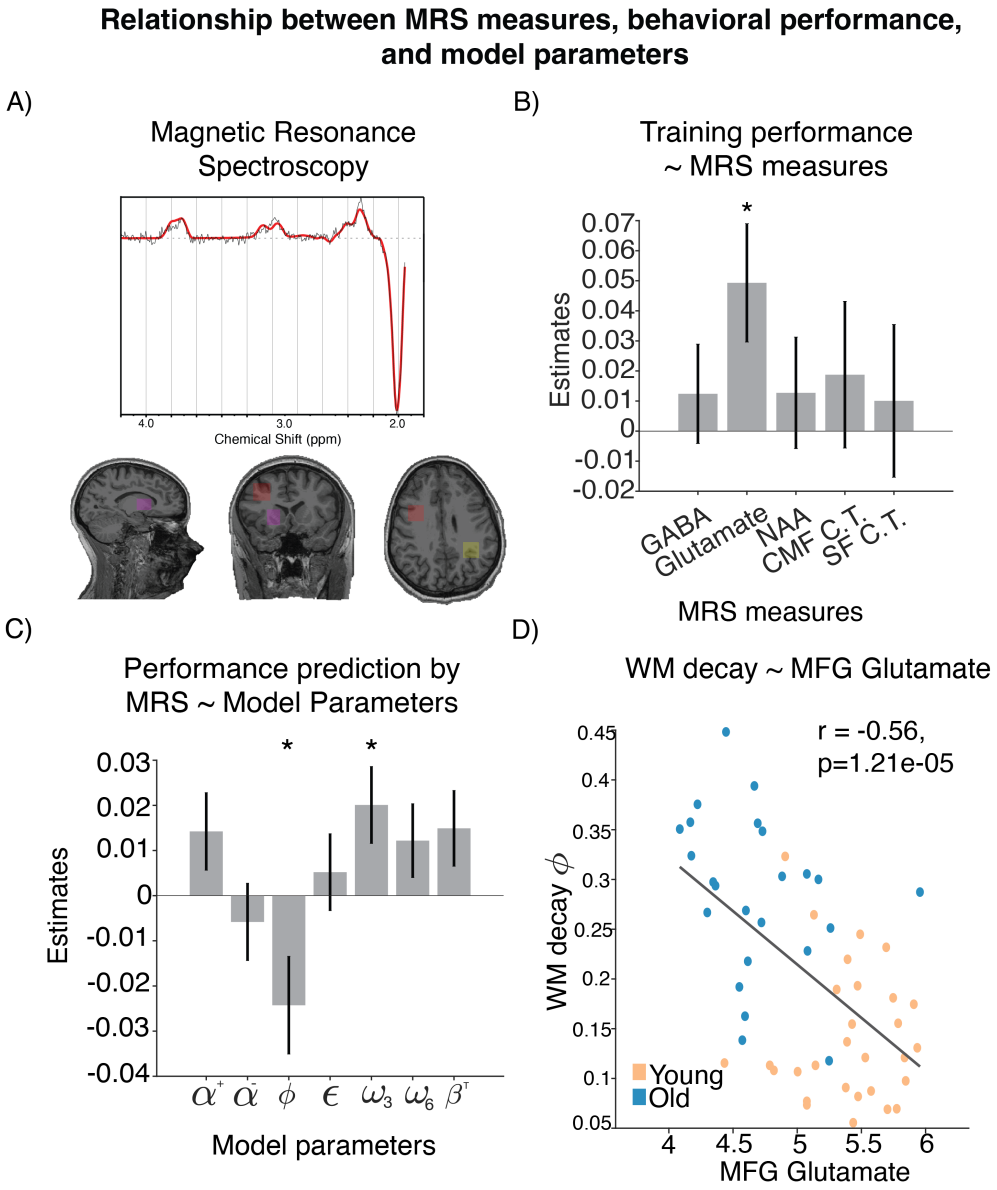

Figure 3: Relationship between MRS measures, performance and model parameters. A) MRS [Fill in the details here]. B) Neural measure predictors that provided best out of sample prediction of learning performance. C) The model with computational model parameters predicting performance predicted values. WM decay and WM weight in set size 3 are the only significant predictors. D) Relationship between WM decay and glutamate levels in MFG.

3 Discussion

Our results suggest that age-related declines in the ability to make decisions from experience are driven by increased forgetting in working memory that is linked to underlying levels of glutamate in prefrontal cortex. Our results provide a computationally specific account of learning impairments that have previously been observed over the course of healthy aging, and also provide insight into its biological underpinnings, in particular suggesting that reduced glutamate impairs the ability of prefrontal recurrent networks to maintain task relevant information over extended periods of time.

While it has long been established that working memory declines over healthy aging (Salthouse and Babcock,

1991), our work shows that these deficits are also at the root of age-related impairments in decisions from experience (Eppinger et al., 2013). Importantly, this result held even when simultaneously accounting for RL contributions to behavior, which have also been theorized to be impacted by cognitive aging (Frank and Kong, 2008; Li et al., 2015). As shown by examples of previous work (A. G. Collins et al., 2014; Leong et al., 2017; Radulescu et al., 2019), it is important to consider interactions between neurocognitive systems rather than studying them in isolation, as this could lead to an incorrect attribution of observed behavioral patterns. Our behavioral modeling results are complementary to those of another recent study that leveraged varying delay between training and testing to examine contributions of working memory, and concluded that older adults engaged WM less than young adults during the short delays. Thus, across studies, there is converging evidence that working memory deficits in older adults can negatively impact decisions from experience, perhaps providing insight into why decisions from description are relatively spared by the cognitive aging process (Li et al., 2015), as such decisions do not typically require working memory. Though our framework provided an ideal setup to disentangle contributions of learning and memory to decisions, one limitation of our task is that it does not provide any behavioral information about why working memory systems fail. For example, higher working memory decay in our model could reflect lower overall memory capacity – but it could also reflect failures to appropriately prioritize storage of task relevant information, including susceptibility to interference effects such as have previously been proposed to play a major role in cognitive aging (Amer et al., 2022). Thus, although our computational approach was able to show that much of the age-related decision making impairment previously attributed to learning is actually attributable to failures of working memory, we rely on future work to better understand the exact computational nature of those failures.

On the biological side, our results suggest that age-related decays in working memory, but no other age-related behavioral changes, were linked to reductions in levels of glutamate in prefrontal cortex. Previous work has noted structural changes in the aging brain, including reduced brain volume and specific reductions in gray matter in certain brain regions, including prefrontal cortex (Buckner et al., 2004; West, 1996). While we did note some structural differences between younger and older participants, these structural changes were not related to decision making, and instead the best neural predictions of task performance relied primarily on neurochemical levels, in particular, glutmate. Glutamate is the primary excitatory neurotransmitter in the brain, and in prefrontal cortex, is thought to support local recurrent signaling that supports the active maintenance of information in cortical neural networks. An enticing interpretation of these results is that our non-invasive MRS measures, which provide regional quantification of glutamate, may provide a readout of changes in the local synaptic architecture (for example, decreased density of excitatory synapses) that play a causal role in the cognitive aging process. That said, a major limitation of MRS is that we are unable to verify that the age-related differences in glutamate that we measure are localized to synapses, or even to neurons. The chemical specificity of our findings lends some support to the idea that glutamate is playing a functional role, rather than simply serving as one of many markers for the metabolic changes that occur over healthy aging, yet additional work leveraging animal models would be necessary to verify this idea and fully elucidate a causal mechanism.

One important limitation of the current study is the cross-sectional design. Specifically, we compared a group of young and older adults, without directly observing age related changes within-subjects (i.e. a longitudinal design). Nonetheless, several aspects of our data suggest that the differences we observed are related to age, rather than other factors that may have differed across our young and older cohorts. First, we collected *The Repeatable Battery for the Assessment of Neuropsychological Status* (RBANS) scores, which revealed that our two groups reflected similar samples of their age-groups with respect to overall cognitive function. Second, task performance decreased with age within the older adult group, rather than simply across the two groups.

We have focused on testing healthy older adults in order to isolate the aging as dimension along which we tested the change in RL and WM. In the future it would also be valuable to examine these changes in clinical populations (i.e. individuals with mild cognitive impairment (MCI) or individuals with Alzheimer's disease/dementia). Testing how neural mechanisms in these neurodegenerative disorders relate to RL/WM would further expand our understanding of the underpinnings of dementia-related symptoms. Furthermore, recognizing the signs of specific impairments at different stage of dementia development could inform cognitive-training programs which have been used to mitigate/delay cognitive symptoms in these neurodegenerative disorders (Clare and Woods, 2003). One interesting related question is that of the dynamics of age-related changes, in particular as to whether the measured age-related neural/cognitive changes are gradual, or characterized by a sudden onset at a critical time point in lifespan? Based on the absence of age-related correlation with performance in young adults, and negative correlation with age within the old group it seems that the relationship between age and cognitive functions might not be linear, and instead begin to decline more rapidly at older ages. Future work employing longitudinal studies could address this question, and potentially link

non-linear declines in neural and behavioral measures to protracted onset of age-related disease.

In summary, we show that age-related declines in the ability to make decisions from experience are driven largely by deficits in the ability to use working memory to guide choice. These behavioral deficits are accompanied by changes in neurochemistry, most notably reductions in prefrontal glutamate levels, that map specifically onto computational markers for working memory impairment, and increase with age. These findings suggest that a major component of age-related changes in decision making could result from reductions in prefrontal excitatory signaling that impair working memory systems necessary to translate recent information into appropriate action.

4 Methods

4.1 Participants

We recruited 78 participants in total (42 older adults - age mean(SD) = 68(8.5); 36 young adults, age mean(SD) = 21(4.4)) for a two session study. Older adults were recruited from the community. Young adults were recruited from the Brown University participant pool or from community the community. Recruitment targeted young adults (18-30) and older adults (60-80), however the inclusion criterion was broader and only required participants to be at least 18 years of age. Visual exclusion criteria for enrollment in the study included 1) direct report of color blindness or poor performance on Ishihara color plates, 2) a best-corrected visual acuity less than 20/40 in both eyes at distance or near, and 3) abnormalities in peripheral vision determined by confrontation visual field testing. Additional exclusion criteria related to the safety of MRI imaging excluded participants with contraindication to MRI including claustrophobia, pregnancy, or metal implants.

During the first session, all participants completed an RL-WM behavioral task as well as additional cognitive testing using the Repeatable Battery for the Assessment of Neurospychological Status (RBANS). During the second session participants underwent MRS and completed additional behavioral testing. Out of 36 young adults, 6 did not complete the MRS session; out of 42 old adults, 18 did not complete the MRS session. These participants were omitted from the analyses which linked behavioral/modeling data and neural measures. The two sessions were separated by a maximum of seven days. Participants received monetary compensation for participating in the study. All participants provided a written informed consent prior to beginning the experiment. All procedures were approved by the Brown University Institutional Review Board under protocol 0812992595 (behavioral session) and 1203000583 (MRS session).

4.2 Task

A general format of reinforcement learning experiments assesses subjects' engagement of the feedback-dependent learning process, which enables them to store rewarding stimulus-response associations. The RL-WM task employs the same logic, while simultaneously manipulating the working memory (WM) involvement by varying the number of stimulus-response associations participants are required to learn in a given block (A. G. Collins, 2018; A. G. Collins and Frank, 2012, 2018; Figure 1). In the previous work, this manipulation yielded a way to disentangle the contribution of WM and RL to the learning process (Master et al., 2020).

Given that WM is capacity limited and susceptible to decay, participants are more likely to have stored in working memory an informative stimulus-action association for a given trial when there are fewer items to store. Since WM enables fast, albeit short lasting and limited storage, we expected the accuracy to asymptote within very few trials - if the number of associations is within the capacity bounds. On the other hand, if the number of associations participants are required to store exceeds their WM capacity, they would be more likely to need to use a more incremental, but more robust system to make a choice (RL). Therefore, having two conditions (small and high set size) enabled us to dissociate the contribution of these two learning systems.

Learning phase: Before starting the actual task, participants received detailed task instructions, and a brief practice phase. They were told that the goal of the experiment was to learn a correct key press in response to the given images, in order to earn as many points as possible. We provided participants with trial examples during which they were presented with a stimulus on the screen - they had 1 second to press one of the three keys, and were subsequently given a 1-s deterministic feedback. If they selected a correct response, participants received a point (+1); if they selected a wrong response key they received 0 points. Participants advanced to the next trial following the feedback termination (Fig: 1A). Points were translated to an incentive payment at the end of the study.

Participants learned in 10 independent blocks, six with small set size (3 stimuli per block) and four with high set size (6 stimuli per block), each block with a novel set of images. There were more small-set size blocks due to the fact that learning fewer stimulus-response associations provides a noisier assessment of the learning performance. In each block, each stimulus had a correct associated action that the participant needed to discover through trial and error (e.g. action 3 is correct for stimulus 1), and appeared 9 times during the block. The stimulus order was pseudo-randomized to ensure a uniform distribution of delay between two successive presentations of the same stimulus (A. G. Collins, 2018). We counterbalanced correct stimulus-response mappings across the blocks.

Testing phase: After the training phase, participants completed an unrelated 20-minute task (Probabilistic selection task (PST); Frank et al., 2004) that was visually distinct from the RL-WM task and served to introduce an extended delay between training and the test phase. After completing the PST task, participants were again tested on their knowledge of the stimulus-response associations learned in the RL-WM training blocks. However, unlike in the training phase, feedback was omitted to prevent new learning. Since choices in the test phase could only be informed by feedback received at least 20 minutes prior, we assume that WM systems cannot contribute to accurate responding in the test phase.

4.3 Computational model

In order to understand the cognitive factors that drive age-related differences in behavior, we used a hybrid reinforcement learning (RL) and working memory (WM) model (RL-WM). This model is designed to disentangle the contributions of RL and WM to learning by accounting for each process in a separate module. The RL module tracks the *values*, Q, of stimulus-action associations, which are learned incrementally from the reward history. The WM module acquires stimulus-action association *weights*, W, through fast, one-shot learning, but its stored associations decay over time. By combining the two modules, the RL-WM model is able to quantify the the relative influence of RL and WM processes on learning (A. G. Collins, 2018; A. G. Collins et al., 2014; A. G. Collins and Frank, 2012).

4.3.1 RL learning rule

The incremental learning of stimulus-action values in the RL module is based on a simple delta rule (Sutton and Barto, 2018). Specifically, on each trial t, the value $Q(s,a)$ of the action a made in response to the presented stimulus s is updated in proportion to the reward prediction error δ (difference between expected and observed outcome):

$$\delta_{\text{RL}} = r - Q_t(s,a)$$

$$Q_{t+1}(s,a) = \begin{cases} Q_t(s,a) + \alpha^+ \delta_{\text{RL}} & \text{if } \delta_{\text{RL}} > 0 \\ Q_t(s,a) + \alpha^- \delta_{\text{RL}} & \text{if } \delta_{\text{RL}} \leq 0 \end{cases}$$

where α^+ and α^- are positive and negative learning rates, and r is the outcome for incorrect and correct trials (0 or 1 point, respectively). Previous work suggests that individuals learn differently from positive and negative feedback, specifically suggesting that they are more likely to neglect negative feedback when learning rewarding responses (Frank et al., 2007; Gershman, 2015; Niv et al., 2012). To address this property of learning, we allow for separate learning rates when updating Q-values, depending on the sign of the prediction error.

Q-values are initialized at $Q_0 = 1/n_A$ (where n_A is the number of possible response actions) at the start of each block. These are uniform values (equal values for all S-A associations) that reflect the reward expectation in the absence of learned information.

4.3.2 WM learning rule

In contrast, the WM module is a one-shot learning system that immediately stores and retains the information from the previous trial. To model this, we quantified WM stimulus-action weights as storing the immediate outcome of the trial:

$$W_{t+1}(s,a) = r \qquad \text{if } \delta_{\text{WM}} > 0$$

The neglect of negative feedback is also assumed to affect WM. To capture this, we allow for imperfect encoding of the outcome as an association weight when the WM module's prediction error is negative. The strength of this

imperfection ν is identical to the relative neglect of negative feedback in the RL module, $\frac{\alpha^-}{\alpha^+}$.

$$W_{t+1}(s,a) = W_t(s,a) + \nu(r - W_t(s,a)) \qquad \text{if } \delta_{\text{WM}} \leq 0$$

However, we note that as the positive and negative learning rates are not subject to any order constraint, ν is permitted to be greater than 1, which would imply a relative preference to learn from negative feedback.

The WM weights are initialized to W_0 which is defined similarly to the initial Q-values, but unlike the Q-values, WM weights are susceptible to decay ϕ. On each trial, the ϕ parameter pulls the WM weights to their initial values W_0:

$$W_{t+1}(s_i,a_j) = W_t(s_i,a_j) + \phi(W_0(s_i,a_j) - W_t(s_i,a_j)) \qquad \forall s_i \forall a_j \neq (s,a)$$

This decay applies to all stimulus-action associations except the exact association seen on the current trial.

4.3.3 Policy

Both the RL and WM modules contribute to the likelihood on each trial of choosing each of the n_A possible actions. To generate an action policy within each module, we transform the Q-values and WM weights separately into choice probabilities:

$$\begin{aligned} P_{\text{RL}}(a|s) &= \frac{\exp(\beta^{\text{L}}\, Q_t(s,a))}{\sum_{i=1}^{n_A} \exp(\beta^{\text{L}}\, Q_t(s,a_i))} \\ P_{\text{WM}}(a|s) &= \frac{\exp(\beta^{\text{L}}\, W_t(s,a))}{\sum_{i=1}^{n_A} \exp(\beta^{\text{L}}\, W_t(s,a_i))} \end{aligned} \tag{1}$$

These softmax policies imply that actions with higher Q-values and WM weights will be selected with higher probability. The inverse temperature β^{L}, which applies to both softmax functions, controls the overall extent to which the overall choice process is deterministic during the learning phase. Higher β^{L} values imply that the process will be more deterministic and less exploratory.

To integrate the RL and WM modules' policies, the RL-WM model assumes that the choice is generated as a function of a weighted mixture of the RL and WM policies, where this proportional weighting is determined by a WM weight ω parameter that quantifies one's relative reliance on WM:

$$P_{\text{RL-WM}}(a|s) = \omega^{n_S}\, P_{\text{WM}}(a|s) + (1 - \omega^{n_S})\, P_{\text{RL}}(a|s)$$

As the number of associations to store exceeds WM's capacity, individuals should rely less on WM and more on RL. To capture this, we allow the relative reliance on each process to depend on the set size n_S. Higher ω^{n_S} values imply greater reliance on WM and lower values imply greater reliance on RL while learning n_S stimulus-action associations.

We further extended the policy to capture random lapses in the choice process. Specifically, individuals often make value-independent, random lapses in action - independent of the learning process. To capture this behavioral property, we added a random noise parameter in choice selection in the final policy: (A. G. Collins and Frank, 2012; Nassar and Frank, 2016):

$$P = (1 - \varepsilon)\, P_{\text{RLWM}} + \varepsilon\, \frac{1}{n_A} \tag{2}$$

where $1/n_A$ is the uniform random policy, and ε is the noise parameter.

4.3.4 Test phase

Given that the test phase is administered with a delay (thus eliminating WM contribution), we assume that the choice process during this phase is exclusively supported by RL. The choice policy is based only on the Q-values learned for the stimulus-action associations at the end of each learning block:

$$\begin{aligned} P_{\text{RL}}^{\text{test}}(a|s) &= \frac{\exp(\beta^{\text{T}}\, Q_t(s,a))}{\sum_{i=1}^{n_A} \exp(\beta^{\text{T}}\, Q_t(s,a_i))} \\ P^{\text{test}} &= (1 - \varepsilon)\, P_{\text{RL}}^{\text{test}} + \varepsilon\, \frac{1}{n_A} \end{aligned}$$

Here, β^T is the inverse temperature specific to the test phase (i.e., different from the learning phase β^L). We also assumed some noise in this decision process, with the same lapse rate ε as in the learning phase (see Eq. 2). Q-values are no longer updated as there is no feedback given during the test phase.

The list of free parameters for the RL-WM model includes a positive learning rate (α^+) and a negative learning rate (α^-), two inverse temperatures (in each phase of the task, β^L and β^T), random lapse rate (ε), decay rate (ϕ), and two degrees of reliance on WM (in each set size condition, ω^3 and ω^6). For every participant, we inferred the value of each of these parameters except β^L, for which we made the simplifying assumption that a singular value applies to all participants in the same age group. Most recent work with the RL-WM model has fixed β^L to the a singular value (often 50 or 100) for all participants (A. G. Collins, 2018; Master et al., 2020); our approach is similar, but ultimately more flexible, as it effectively allows the data to dictate what value to fix for β^L.

A schematic representation of how the RL-WM process generates behavioral data in both the learning and testing phases of the RL-WM task is presented in Figure 2A.

4.3.5 Hierarchical Bayesian formulation of the RL-WM model

To estimate the parameters of the RL-WM model for all participants simultaneously, we developed the first hierarchical Bayesian formulation of the RL-WM model. This Bayesian implementation is a novel extension of the RL-WM model, allowing for to the inclusion of domain knowledge directly in the model (via carefully developed priors) and the incorporation of theoretically meaningful hierarchical structure. A hierarchical Bayesian approach to model fitting offers many benefits, including the ability to quantify the uncertainty in each parameter estimate and the regularization of extreme estimates with respect to the group (for an introduction, see Lee, 2011).

We compared three versions of the Bayesian RL-WM model with different hierarchical structures. First, we defined a non-hierarchical model by specifying a prior for each unobserved parameter of the RL-WM model's data-generating process (as described above). This would be equivalent to fitting the model separately to each participant's data, were it not for our simplifying assumption that the same value of β^L is used for all participants. Next, we considered a hierarchical extension of the model over participants, such that all P participants' parameter values (e.g., all 78 learning rates, $\alpha_1, \alpha_2, \ldots, \alpha_P$) are assumed to be drawn from a group-level distribution (e.g., $\alpha_p \sim \text{Beta}(1+a, 1+b)\ \forall p$). Finally, we considered a model with separate hierarchies over the participants within each age group. This version of the RL-WM includes different hyperparameters for each age group (e.g., a_{young}, b_{young} vs. a_{older}, b_{older}), which would allow us to make inferences about group-level differences in each dynamic of the RL-WM process.

For each version of the model, we specified priors for participant-level parameters and hyperpriors for group-level hyperparameters that were mildly to moderately informative. The priors and hyperpriors used to specify the winning two-group model are detailed in the Supplement. Prior predictive checks and other simulation-based procedures were used to confirm that the set of prior distributions and the RL-WM model likelihood taken together specified a reasonable model (Baribault and Collins, 2022; Kennedy et al., 2019; see Fig. S1).

4.3.6 Model fitting

For each of the three candidate models, we used Stan (Carpenter et al., 2017) to estimate the joint posterior distribution of all model parameters via Markov chain Monte Carlo (MCMC) sampling. After running a model with 4 chains of 500 warmup iterations and 1500 kept iterations each, we performed a series of diagnostic checks in accordance with current best practices for MCMC methods (Betancourt, 2016; Gelman et al., 2013; Vehtari et al., 2021). We required an $\hat{R}$ value of ≤ 1.01 and an effective sample size ≥ 400 for all parameters, a BFMI of ≥ 0.2 for all chains, and that no divergences were observed. Only kept iterations from model output that met these criteria were used for analysis.

We used WAIC (widely applicable or Watanabe-Akaike information criterion Watanabe, 2010) as our model comparison metric as it is fully Bayesian, invariant to parameterization, and straightforward to compute. Because response data from successive trials of the RL-WM task are not independent, we consider one block of data from one participant as the smallest unit of data when computing log likelihood for WAIC. As WAIC is an estimate of out-of-sample prediction error, lower WAIC values indicate a better model. Our final model selection was further supported by posterior predictive checks of the models' relative descriptive adequacy (see Fig. S2).

In the model-based analyses reported here, all intervals are 95% equal-tailed credible intervals (CrI), unless otherwise specified. Additional details about our model-based analysis procedures and checks are included in the Supplement.

4.4 MRS procedure

Glutamate and GABA levels were measured in three brain regions (striatum, middle frontal gyrus [MFG], and intraparietal sulcus [IPS]) using magnetic resonance spectroscopy (MRS). First, structural images of the participant brain were acquired using a high-resolution T1-weighted sequence (MPRAGE, TR/TE/TI = 1,900/3.02/900 ms, 9° flip angle, 1.0 x 1.0 x 1.0 mm3 voxel resolution) with a 64-channel RF receive coil array on a 3T MRI scanner (Siemens MAGNETOM Prisma). Next, we manually placed voxel bounding boxes in each brain region for MRS data acquisitions. The striatal voxel was 18 x 24 x 15 mm and was placed such that the anterior portion of the voxel started at the anterior extreme of the head of the caudate and that it extended posterior to maximize inclusion of caudate and putamen and minimize inclusion of ventricular space. A 20 mm cubic voxel was placed in the right MFG immediately anterior to the precentral sulcus and immediately inferior to the superior frontal sulcus. A 20 mm cubic voxel was placed to be centered at the anterior-ventral section of the left IPS. Representative images of voxel placements are available in Fig. 3.

For each voxel, we acquired measures of GABA using a MEGA-PRESS sequence (Hu et al., 2013) (TR = 1,500 ms, TE = 68 ms, average = 192) with double-banded pulses, which were used to simultaneously suppress water signal and edit the γ-CH2 resonance of GABA at 3 ppm. Linear and 2nd order shimming was used to achieve typical linewidth ($\sim$ 14Hz). Difference spectra were obtained by subtracting the signals obtained from the selective double-banded pulse applied at 1.9 and 4.7 ppm ('Edit on') from those obtained from the double-banded pulse applied at 4.7 and 7.5 ppm ('Edit off'). Glutamate scans were conducted using the PRESS sequence (Hancu, 2009) (TR = 3,000 ms, TE = 30 ms, 90° flip angle, average = 64). A variable pulse power and optimized relaxation delays (VAPOR) technique was used in both sequences to achieve water suppression (Tkáč et al., 1999). While MRS data was collected, participants completed a simple task that required them to push a button whenever a fixation point changed color (Shibata et al., 2017).

Glutamate was quantified using LC-model (Provencher, 2001), which attempts to fit the average signal in the frequency domain using a linear combination of basis functions. Separate basis functions were used to quantify glutamate and glutamine, a molecule that has similar spectral characteristics to glutamate in the PRESS sequence. The reliability of glutamate quantifications was indicated by the Cramer-Rao lower bounds and a criterion of 20 % was chosen to reject low-quality signal, however no measurements were rejected due to this criterion.

GABA was quantified using a custom peak integration process implemented in Matlab. This quantification procedure was used because it produced higher split half reliability on our dataset than standard GABA quantification software (Edden et al., 2014). Raw data was obtained from the Siemens Prisma scanner in the form of the so-called 'twix' file which contains the (complex) individual signals from each receive channel for every average. Signals underwent phase shifting to equalize the starting phase of all of the receive channel signals prior to combining for each signal average. Signals were combined using weighting factors based on individual signal amplitudes. Starting with the highest amplitude signal, channels were added until there was no further increase in NAA peak SNR. Free induction decays were averaged separately for "off" and "on" pulse conditions and subtracted to produce a difference signal. The difference signal was transformed into frequency space with a fast fourier transform and frequencies were converted to parts per million, where 1 PPM is equal to 123.255 MHz, and relative to a water reference of 4.8 PPM. The GABA peak was quantified by integrating chemical shifts ranging from 2.9 to 3.1 ppm and subtracting out the integrated signal in a surrounding reference window (2.8-2.9, 3.1-3.2 ppm). This procedure was validated through split half correlations in which the entire procedure was performed separately for odd and even acquisition volumes and resulting GABA measurements for odd and even acquisitions were correlated with one another to yield relatively high reliability for MFG and IPS measures (R= 0.80 for both regions) and moderate reliability for striatal GABA measures (R=0.68; see supplementary Fig. S6).

Freesurfer 6.0 was used to reconstruct T1 anatomical scans from dicom images collected using the MPRAGE sequence following the recon-all -all pipeline. The initial pial surface outputs were manually corrected for brainmasks that included skull tissues as described in the Freesurfer quality control documentation (https://freesurfer.net/fswiki). Next, partial volume fractions for gray matter (cortex + subcortical), white matter, and cerebrospinal fluid were computed as voxel maps using the mri_compute_volume_fractions Freesurfer command based on the edited T1 reconstruction. Then, masks for the three brain regions (striatum, MFG, and IPS) measured with MRS were constructed using the Gannet 2.1 toolbox (Edden et al., 2014) based on the voxel bounding boxes manually placed during the MRS acquisition. Gray/white matter volumes in each region was computed by summing partial volume voxel maps with masking. Similarly, anatomical measures within each region were obtained by summing tissue maps with masking using the mri_segstats Freesurfer command on labelled parcellation of the cortex using the Desikan-Killiany atlas

(Desikan et al., 2006) and automatic segmentation of the subcortical structures (Fischl et al., 2002).

4.5 Behavioral analyses

To visualize participants' learning trajectory, we created learning curves by collapsing participants' accuracy at each stimulus iteration. This enabled us to separate early learning and asymptotic performance (late learning accuracy). Trials with missing responses (i.e., where participants did not respond within the time limit) were excluded from analyses.

While learning curves are useful for visualizing learning trajectory, they cannot be used to make inferences about trial-by-trial contribution of different factors (i.e. related to RL or WM) to participants' accuracy. Thus, to quantify performance in terms of factors related to RL and WM we ran a trial-by-trial analysis using a mixed-effects general linear model (GLM), predicting accuracy (coded as 0 or 1 on each trial). Specifically, the predictors in the logistic regression consisted of the following: set size (the number of associations), delay (number of intermediate trials between two successive rewarded stimulus representations), and reward history (stimulus-dependent cumulative reward history). We also added trial and block number predictors, to control for overall improvement across the task. We used participants' coefficients to predict their respective age using a linear model, in order to draw a relationship between age and RL and WM-related factors effect on performance. We excluded coefficients from 2 participants, as these coefficients were over 2 standard deviations above the mean following the approach implemented in previous work (Master et al., 2020).

4.6 Data-driven approach to identifying best MRS predictors

To examine the effect of brain measures on the parameters and task performance, we first had to reduce the dimensionality of highly-correlated MRS data by identifying the best set of MRS predictors in explaining participants' learning performance. We focused on learning performance because unlike the test phase the learning phase contains signatures of both WM and RL. We constructed a GLM to predict learning performance using structural (gray matter and cortical thickness in SF,CMF and RMF cortex) and neurochemical (glutamate, GABA, NAA) measures. Next, we used a *k*-fold cross-validation approach to identify the best configuration of predictors that minimizes the loss (mean squared error) in out-of-sample prediction. We randomly sampled 4/5 of the data to train the model, leaving out the remaining 1/5 of the data for validation, repeating this process 200 times. On each of the 200 iterations we stored the best configuration of predictors that minimized the loss of the model's prediction of the out-of-sample performance. We also added the regularization term, which represented a combination of L^1 and L^2 penalty (i.e. elastic net; with alpha = .5 such that ridge (L^2) and lasso (L^1) optimization are weighted equally; regularization coefficient λ was set to default - lasso sets the maximum value of λ that gives a non-null model) to help us eliminate the predictors that did not significantly contribute to performance and might lead to overfitting.

5 Acknowledgments

This work was supported by National Institute on Aging grants K99AG054732 and R00AG054732 to MRN. We thank Rachel Rac-Lubashevsky and Michael Frank for helpful comments.

References

Amer, T., Wynn, J. S., & Hasher, L. (2022). Cluttered memory representations shape cognition in old age. *Trends in Cognitive Sciences*.

Andersen, R. A., & Buneo, C. A. (2002). Intentional maps in posterior parietal cortex. *Annual review of neuroscience*, *25*, 189–220.

Baribault, B., & Collins, A. (2022). Troubleshooting bayesian cognitive models.

Betancourt, M. (2016). Diagnosing suboptimal cotangent disintegrations in Hamiltonian Monte Carlo. *arXiv preprint arXiv:1604.00695*.

Buckner, R. L., Head, D., Parker, J., Fotenos, A. F., Marcus, D., Morris, J. C., & Snyder, A. Z. (2004). A unified approach for morphometric and functional data analysis in young, old, and demented adults using automated atlas-based head size normalization: Reliability and validation against manual measurement of total intracranial volume. *Neuroimage*, *23*(2), 724–738.

Carpenter, B., Gelman, A., Hoffman, M. D., Lee, D., Goodrich, B., Betancourt, M., Brubaker, M., Guo, J., Li, P., & Riddell, A. (2017). Stan: A probabilistic programming language. *Journal of Statistical Software*, *76*(1).

Cattell, R. B. (1943). The measurement of adult intelligence. *Psychological bulletin*, *40*(3), 153.

Chowdhury, R., Guitart-Masip, M., Lambert, C., Dayan, P., Huys, Q., Düzel, E., & Dolan, R. J. (2013). Dopamine restores reward prediction errors in old age. *Nature neuroscience*, *16*(5), 648–653.

Clare, L., & Woods, B. (2003). Cognitive rehabilitation and cognitive training for early-stage alzheimer's disease and vascular dementia. *Cochrane database of systematic reviews*, (4).

Collins, A. G. (2018). The tortoise and the hare: Interactions between reinforcement learning and working memory. *Journal of cognitive neuroscience*, *30*(10), 1422–1432.

Collins, A. G., Brown, J. K., Gold, J. M., Waltz, J. A., & Frank, M. J. (2014). Working memory contributions to reinforcement learning impairments in schizophrenia. *Journal of Neuroscience*, *34*(41), 13747–13756.

Collins, A. G., & Frank, M. J. (2012). How much of reinforcement learning is working memory, not reinforcement learning? a behavioral, computational, and neurogenetic analysis. *European Journal of Neuroscience*, *35*(7), 1024–1035.

Collins, A. G., & Frank, M. J. (2014). Opponent actor learning (opal): Modeling interactive effects of striatal dopamine on reinforcement learning and choice incentive. *Psychological review*, *121*(3), 337.

Collins, A. G., & Frank, M. J. (2018). Within-and across-trial dynamics of human eeg reveal cooperative interplay between reinforcement learning and working memory. *Proceedings of the National Academy of Sciences*, *115*(10), 2502–2507.

Desikan, R. S., Ségonne, F., Fischl, B., Quinn, B. T., Dickerson, B. C., Blacker, D., Buckner, R. L., Dale, A. M., Maguire, R. P., Hyman, B. T., et al. (2006). An automated labeling system for subdividing the human cerebral cortex on mri scans into gyral based regions of interest. *Neuroimage*, *31*(3), 968–980.

Dumitriu, D., Hao, J., Hara, Y., Kaufmann, J., Janssen, W. G., Lou, W., Rapp, P. R., & Morrison, J. H. (2010). Selective changes in thin spine density and morphology in monkey prefrontal cortex correlate with aging-related cognitive impairment. *Journal of Neuroscience*, *30*(22), 7507–7515.

Durstewitz, D., Seamans, J. K., & Sejnowski, T. J. (2000). Dopamine-mediated stabilization of delay-period activity in a network model of prefrontal cortex. *Journal of neurophysiology*.

Eckstein, M. K., Master, S. L., Xia, L., Dahl, R. E., Wilbrecht, L., & Collins, A. G. (2022). The interpretation of computational model parameters depends on the context. *BioRxiv*, 2021–05.

Edden, R. A., Puts, N. A., Harris, A. D., Barker, P. B., & Evans, C. J. (2014). Gannet: A batch-processing tool for the quantitative analysis of gamma-aminobutyric acid–edited mr spectroscopy spectra. *Journal of Magnetic Resonance Imaging*, *40*(6), 1445–1452.

Eppinger, B., Schuck, N. W., Nystrom, L. E., & Cohen, J. D. (2013). Reduced striatal responses to reward prediction errors in older compared with younger adults. *Journal of Neuroscience*, *33*(24), 9905–9912.

Fischl, B., Salat, D. H., Busa, E., Albert, M., Dieterich, M., Haselgrove, C., Van Der Kouwe, A., Killiany, R., Kennedy, D., Klaveness, S., et al. (2002). Whole brain segmentation: Automated labeling of neuroanatomical structures in the human brain. *Neuron*, *33*(3), 341–355.

Frank, M. J., & Kong, L. (2008). Learning to avoid in older age. *Psychology and aging*, *23*(2), 392.

Frank, M. J., Moustafa, A. A., Haughey, H. M., Curran, T., & Hutchison, K. E. (2007). Genetic triple dissociation reveals multiple roles for dopamine in reinforcement learning. *Proceedings of the National Academy of Sciences*, *104*(41), 16311–16316.

Frank, M. J., Seeberger, L. C., & O'reilly, R. C. (2004). By carrot or by stick: Cognitive reinforcement learning in parkinsonism. *Science*, *306*(5703), 1940–1943.

Gelman, A., Carlin, J. B., Stern, H. S., Dunson, D. B., Vehtari, A., & Rubin, D. B. (2013). Bayesian Data Analysis.

Gershman, S. J. (2015). Do learning rates adapt to the distribution of rewards? *Psychonomic bulletin & review*, *22*(5), 1320–1327.

Goldman-Rakic, P. S. (1995). Cellular basis of working memory. *Neuron*, *14*(3), 477–485.

Grogan, J., Isotalus, H., Howat, A., Irigoras Izagirre, N., Knight, L., & Coulthard, E. (2019). Levodopa does not affect expression of reinforcement learning in older adults. *Scientific reports*, *9*(1), 1–10.

Hämmerer, D., Li, S.-C., Müller, V., & Lindenberger, U. (2011). Life span differences in electrophysiological correlates of monitoring gains and losses during probabilistic reinforcement learning. *Journal of Cognitive Neuroscience*, *23*(3), 579–592.

Hancu, I. (2009). Optimized glutamate detection at 3t. *Journal of Magnetic Resonance Imaging: An Official Journal of the International Society for Magnetic Resonance in Medicine*, *30*(5), 1155–1162.

Hu, Y., Chen, X., Gu, H., & Yang, Y. (2013). Resting-state glutamate and gaba concentrations predict task-induced deactivation in the default mode network. *Journal of Neuroscience*, *33*(47), 18566–18573.

Kennedy, L., Simpson, D., & Gelman, A. (2019). The experiment is just as important as the likelihood in understanding the prior: A cautionary note on robust cognitive modeling. *Computational Brain & Behavior*, *2*(3), 210–217.

Kruschke, J. K., & Liddell, T. M. (2018). The Bayesian New Statistics: Hypothesis testing, estimation, meta-analysis, and power analysis from a bayesian perspective. *Psychonomic bulletin & review*, *25*(1), 178–206.

Lee, M. D. (2011). How cognitive modeling can benefit from hierarchical Bayesian models. *Journal of Mathematical Psychology*, *55*(1), 1–7.

Leong, Y. C., Radulescu, A., Daniel, R., DeWoskin, V., & Niv, Y. (2017). Dynamic interaction between reinforcement learning and attention in multidimensional environments. *Neuron*, *93*(2), 451–463.

Li, Y., Gao, J., Enkavi, A. Z., Zaval, L., Weber, E. U., & Johnson, E. J. (2015). Sound credit scores and financial decisions despite cognitive aging. *Proceedings of the National Academy of Sciences*, *112*(1), 65–69.

Master, S. L., Eckstein, M. K., Gotlieb, N., Dahl, R., Wilbrecht, L., & Collins, A. G. (2020). Disentangling the systems contributing to changes in learning during adolescence. *Developmental cognitive neuroscience*, *41*, 100732.

Nassar, M. R., & Frank, M. J. (2016). Taming the beast: Extracting generalizable knowledge from computational models of cognition. *Current opinion in behavioral sciences*, *11*, 49–54.

Niv, Y., Edlund, J. A., Dayan, P., & O'Doherty, J. P. (2012). Neural prediction errors reveal a risk-sensitive reinforcement-learning process in the human brain. *Journal of Neuroscience*, *32*(2), 551–562.

Provencher, S. W. (2001). Automatic quantitation of localized in vivo 1h spectra with lcmodel. *NMR in Biomedicine: An International Journal Devoted to the Development and Application of Magnetic Resonance In Vivo*, *14*(4), 260–264.

Radulescu, A., Daniel, R., & Niv, Y. (2016). The effects of aging on the interaction between reinforcement learning and attention. *Psychology and aging*, *31*(7), 747.

Radulescu, A., Niv, Y., & Ballard, I. (2019). Holistic reinforcement learning: The role of structure and attention. *Trends in cognitive sciences*, *23*(4), 278–292.

Randolph, C., Tierney, M. C., Mohr, E., & Chase, T. N. (1998). The repeatable battery for the assessment of neuropsychological status (rbans): Preliminary clinical validity. *Journal of clinical and experimental neuropsychology*, *20*(3), 310–319.

Salthouse, T. A., & Babcock, R. L. (1991). Decomposing adult age differences in working memory. *Developmental psychology*, *27*(5), 763.

Samanez-Larkin, G. R., Worthy, D. A., Mata, R., McClure, S. M., & Knutson, B. (2014). Adult age differences in frontostriatal representation of prediction error but not reward outcome. *Cognitive, Affective, & Behavioral Neuroscience*, *14*(2), 672–682.

Shibata, K., Sasaki, Y., Bang, J. W., Walsh, E. G., Machizawa, M. G., Tamaki, M., Chang, L.-H., & Watanabe, T. (2017). Overlearning hyperstabilizes a skill by rapidly making neurochemical processing inhibitory-dominant. *Nature neuroscience*, *20*(3), 470–475.

Sutton, R. S., & Barto, A. G. (2018). *Reinforcement learning: An introduction*. MIT press.

Tkáč, I., Starčuk, Z., Choi, I.-Y., & Gruetter, R. (1999). In vivo 1h nmr spectroscopy of rat brain at 1 ms echo time. *Magnetic Resonance in Medicine: An Official Journal of the International Society for Magnetic Resonance in Medicine*, *41*(4), 649–656.

Van Vugt, B., van Kerkoerle, T., Vartak, D., & Roelfsema, P. R. (2020). The contribution of ampa and nmda receptors to persistent firing in the dorsolateral prefrontal cortex in working memory. *Journal of Neuroscience*, *40*(12), 2458–2470.

Vehtari, A., Gelman, A., Simpson, D., Carpenter, B., & Bürkner, P.-C. (2021). Rank-normalization, folding, and localization: An improved rhat for assessing convergence of MCMC (with Discussion). *Bayesian analysis*, *16*(2), 667–718.

Wang, M., Gamo, N. J., Yang, Y., Jin, L. E., Wang, X.-J., Laubach, M., Mazer, J. A., Lee, D., & Arnsten, A. F. (2011). Neuronal basis of age-related working memory decline. *Nature*, *476*(7359), 210–213.

Watanabe, S. (2010). Asymptotic equivalence of Bayes cross validation and widely applicable information criterion in singular learning theory. *Journal of machine learning research*, *11*(12).
West, R. L. (1996). An application of prefrontal cortex function theory to cognitive aging. *Psychological bulletin*, *120*(2), 272.
Wong, K.-F., & Wang, X.-J. (2006). A recurrent network mechanism of time integration in perceptual decisions. *Journal of Neuroscience*, *26*(4), 1314–1328.
Yoo, A. H., & Collins, A. G. (2022). How working memory and reinforcement learning are intertwined: A cognitive, neural, and computational perspective. *Journal of Cognitive Neuroscience*, *34*(4), 551–568.

6 Supplements

6.1 Model specification

The data distribution for the two-group Bayesian RL-WM model (i.e., the model used for all of our model-based analyses) is described in full detail in the main text of the paper. We include all prior distributions here to complete the hierarchical Bayesian model specification.
We set the following priors on participant-level parameters:

$$\begin{aligned}
\alpha_p^+ &\sim \text{Beta}(1+a_{g|p}^{\alpha^+}, 1+b_{g|p}^{\alpha^+}) \\
\alpha_p^- &\sim \text{Beta}(1+a_{g|p}^{\alpha^-}, 1+b_{g|p}^{\alpha^-}) \\
\phi_p &\sim \text{Beta}(1+a_{g|p}^{\phi}, 1+b_{g|p}^{\phi}) \\
\omega_p^3 &\sim \text{Beta}(1+a_{g|p}^{\omega^3}, 1+b_{g|p}^{\omega^3}) \\
\omega_p^6 &\sim \text{Beta}(1+a_{g|p}^{\omega^6}, 1+b_{g|p}^{\omega^6}) \\
\varepsilon_p &\sim \text{Beta}(1+a_{g|p}^{\varepsilon}, 1+b_{g|p}^{\varepsilon}) \\
\beta_p^T &\sim \text{Gamma}(1+\alpha_{g|p}^{\beta^T}, \beta_{g|p}^{\beta^T})
\end{aligned}$$

The subscript p indicates that identical priors were set $\forall\ p = 1, 2, \ldots, P$ participants.
The subscript $g|p$ indicates use of the hyperparameter corresponding to the group membership of that participant (where $g = 1$ and $g = 2$ denote the young and old age groups, respectively).

We set the following prior on both β^L parameters:

$$\beta_g^L \sim \text{Gamma}(5, 0.4)$$

The subscript g indicates that this same prior was used for the β^L parameters specific to each of the two age groups.

We set the following hyperpriors on group-level parameters:

$$\begin{aligned}
a_g^{\alpha^+} &\sim \text{Gamma}(1,1) & a_g^{\phi} &\sim \text{Gamma}(1,1) & a_g^{\omega^3} &\sim \text{Gamma}(2,1) & & \\
b_g^{\alpha^+} &\sim \text{Gamma}(4,1) & b_g^{\phi} &\sim \text{Gamma}(2,1) & b_g^{\omega^3} &\sim \text{Gamma}(1,1) & \alpha_g^{\beta^T} &\sim \text{Gamma}(6,1) \\
a_g^{\alpha^-} &\sim \text{Gamma}(1,1) & b_g^{\varepsilon} &\sim \text{Gamma}(1,1) & a_g^{\omega^6} &\sim \text{Gamma}(2,1) & \beta_g^{\beta^T} &\sim \text{Gamma}(3,2) \\
b_g^{\alpha^-} &\sim \text{Gamma}(4,1) & b_g^{\varepsilon} &\sim \text{Gamma}(12,1) & b_g^{\omega^6} &\sim \text{Gamma}(1,1) & &
\end{aligned}$$

The subscript g indicates that this same prior was used for both age groups.
For any pairs of parameters that we considered comparing directly, we ensured that these comparisons would not be biased by any potential lingering influence of the prior by specifying identical hyperpriors. Such pairs include the learning rates, α^+ and α^-, and the mixture parameters, ω^3 and ω^6.

As these hyperparameters are not readily interpretable, we derived group-level means and standard deviations for each RL-WM model parameter post hoc, sample-by-sample.

6.2 Prior predictive checks

To ensure models as-specified were capable and reasonable as models of RL-WM task data, we performed prior predictive checks (Baribault and Collins, 2022). We generated prior predictive distributions by randomly drawing group-level parameter values directly from the hyperpriors, using those values to draw participant-level parameter values directly from the priors, and using those parameter values to simulate a data set with the same experimental design as we used in our behavioral data collection (six $n_S = 3$ blocks and three $n_S = 6$ blocks; 9 iterations per stimulus in each block and in the test phase; three possible response actions). 100 prior predictive datasets were simulated for the prior predictive checks shown here.

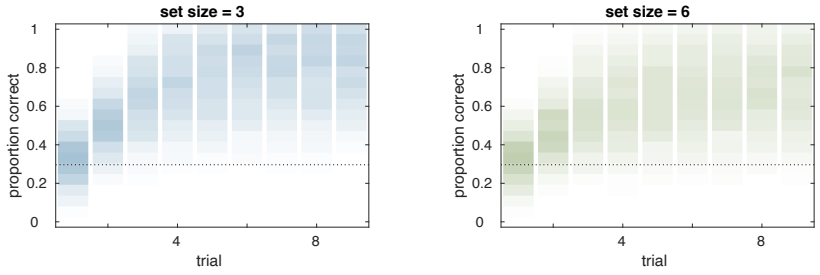

Figure S1: Prior predictive checks for the hierarchical Bayesian RL-WM model. The distribution of learning curves in each set size condition that are implied solely by the model specification suggest the model specification is suitable for the RL-WM task data. Group-level learning curves we would never expect to see (e.g., anti-learning) are not given any notable prior weight; while all possible group-level learning curves we could conceivably observe are given some prior predictive weight, and the most likely learning curves are not excessively strongly weighted. Furthermore, it is nice to see that the set-size effect is an emergent property of our model specification.

6.3 Posterior predictive checks

After model fitting, we performed posterior predictive checks to check the descriptive adequacy of each candidate Bayesian RL-WM model. To generate the posterior predictive distribution, we used the last 500 samples collected (i.e., the last 125 iterations from each chain). Each of these samples from the joint posterior parameter was used to generate a new dataset using an identical experiment structure (same number of participants, same stimulus sequences, etc.).

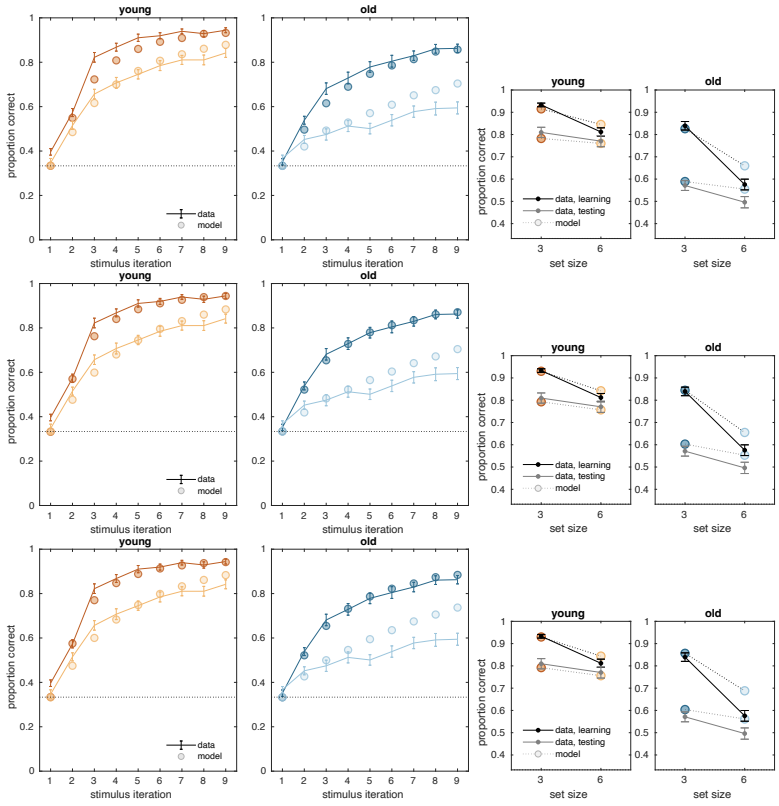

Figure S2: Posterior predictive checks for learning curves (left) and asymptotic means (right) for the non-hierarchical (top row), single-group (middle row), and two-group (bottom row) versions of the Bayesian RL-WM model. (Note that all model-based analyses reported in the main text are based on output from the winning two-group version of the model.)

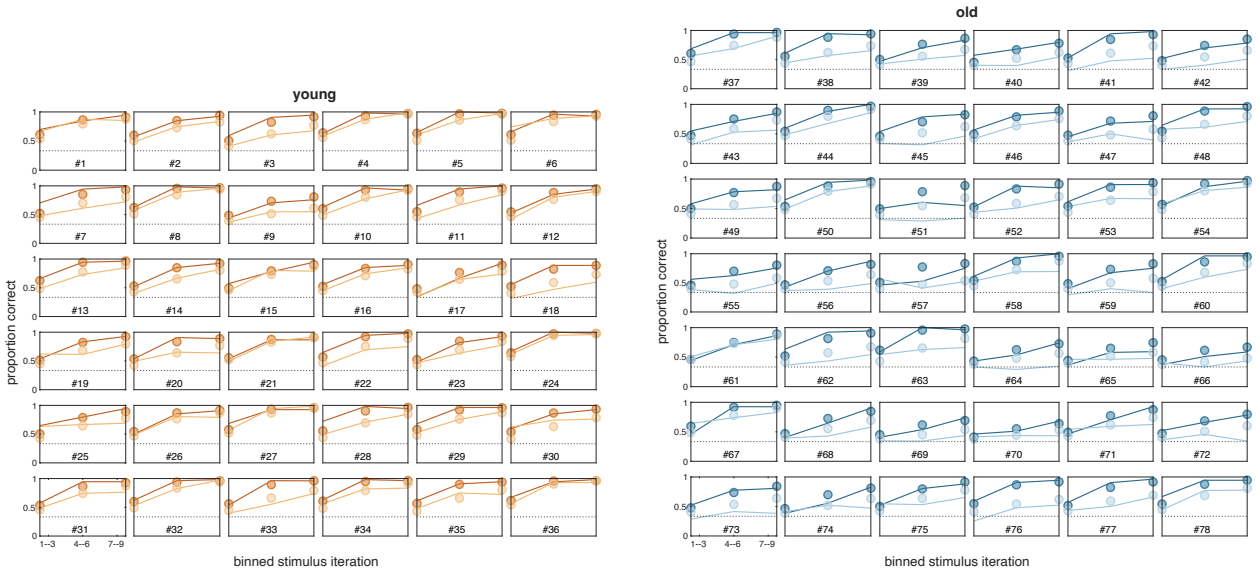

Figure S3: Posterior predictive checks of learning curves for each participant for the two-group version of the Bayesian RL-WM model. As a smaller amount of data is available for individual participants, we plot the curve over stimulus iteration bins (of three iterations each). Our Bayesian RL-WM model captures the performance very well for nearly all participants in the young age group and for many participants in the older age group. Some participants in the older age group are not fit as well, such as #63, and a few are severely misfit, such as #51.

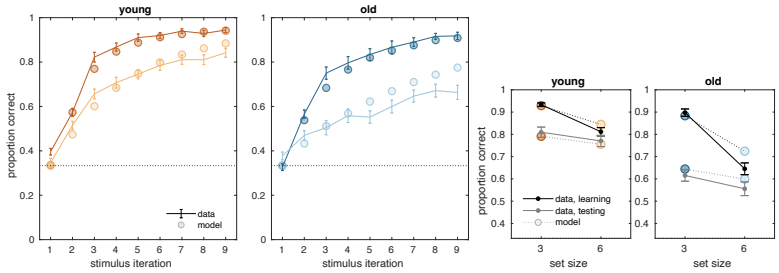

Figure S4: Posterior predictive checks for the two-group version of the Bayesian RL-WM model when data from 14 participants was excluded. The criterion for exclusion was that mean accuracy on at least one set size 3 block was at or below chance when missed responses were classed as incorrect (which is *only* the case for this analysis).

Further exploration of the data suggested that weaker descriptive adequacy of the two-group Bayesian RL-WM model with respect to the the older adults' performance in the set size 6 condition (Fig. S2, bottom row) might be the result of participants' use of a heuristic strategy to reduce the demands of the task, in which they learns only a subset of the stimuli. Specifically, we occasionally observed blocks where the participant had only learned the correct response for a subset of the stimuli, and completely neglected to learn the other associations, and this pattern was evident largely for older adults only. If older adults were using this reducing strategy excessively to ameliorate the considerable difficulty of the set size 6 condition, it could explain the discrepancy as there is no means for this RL-WM model to capture such a severe effect of stimulus identity. Because the model predicts highly similar performance for all stimuli within a block, it cannot capture the performance of participants who rely on employ this strategy more often. We repeated the the posterior predictive check for this model with 14 participants who may have used this heuristic strategy excluded (Fig. S4) as a preliminary assessment whether this might be the case.
If use of this strategy is only evident for older adults for set size 6 blocks, excluding participants who are likely using the reduction strategy in fairly should notably reduce the misfit. This is exactly what we observe in Figure S4 above (despite using only set size 3 performance in establishing a criterion). The heuristic strategy on at least one $n_S = 3$ block greatly improved the posterior predictive check performance in the older adult group, particularly in set size 6. This supports our conjecture that excessive use of alternative strategies can affect model adequacy in the RL-WM task. Further assessment of the robustness of RL-WM models to contaminant response patterns is beyond the scope of the present work.

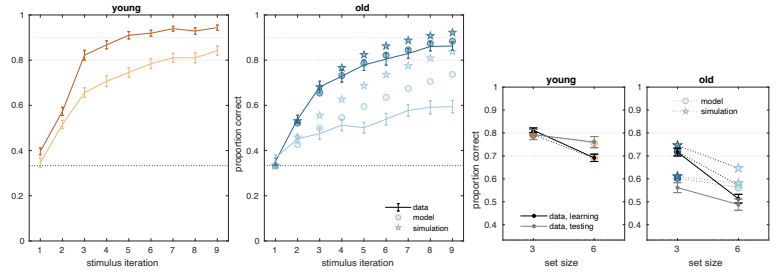

Figure S5: Exploratory demonstration of the role of decay rate ϕ in older adults' performance. Posterior predictive checks were recomputed after replacing the posterior samples for individual-level decay parameters for all older adults group with the posterior samples for the group-level decay rate of the young adults. While these simulation results are not sufficient as the basis for a quantitative measure or test, examining the difference in the RL-WM model's behavioral predictions before (circles) and after (stars) this substitution is revealing: It suggests the lower decay rate might be responsible for most of the difference in behavioral performance between the age groups during the learning phase, particularly for set size 3. Decay rate can recover less of the group difference during the test phase (as the test-phase inverse temperature β^T exerts stronger control in this portion of the RL-WM model). Lighter dotted lines are included to facilitate comparison across groups; the black dotted lines represent chance performance.

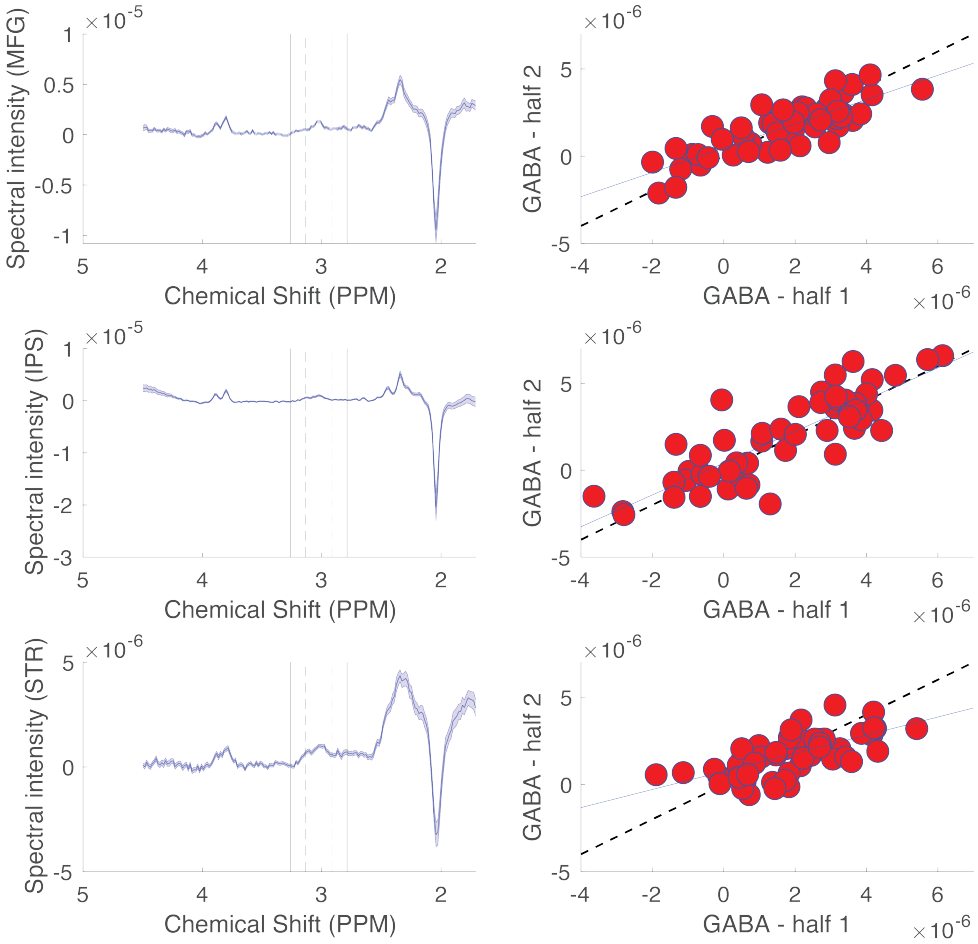

Figure S6: Description and validation of GABA quantification methods. The GABA peak in megaPRESS difference spectra was quantified by integrating chemical shifts ranging from 2.9 to 3.1 ppm and subtracting out the integrated signal in a surrounding reference window (2.8-2.9, 3.1-3.2 ppm). The reliability of this quantification method in our dataset was tested by splitting megaPRESS data into two halves, the first corresponding to the "odd" difference spectra and the second corresponding to the "even" difference spectra. Split half correlations between peak integrals for the two halves served to measure the reliability of our analysis method. Left: Averaged difference spectra for the three brain regions: middle frontal gyrus (top), intraparietal sulcus (middle), and striatum (bottom). Dotted vertical lines mark the edges of the integration window, whereas solid vertical lines mark the edges of the refernce window. Right: split half correlations for each brain region (top = MFG, middle = IPS, bottom = STR) were relatively high (R = 0.8, 0.8, 0.68 respectively for the three regions). GABA quantification on even trials (ordinate) is plotted against GABA quantification on odd trials (abscissa) for each participant (red points). Dotted line reflects the unity line and solid line reflects a least squares linear fit.